Application of fluid dynamic gauging to annular test apparatuses for studying fouling and cleaning

T. Gu[1], F. Albert[2], W. Augustin[2], Y.M.J. Chew[3], M. Mayer[2], W.R. Paterson[1], S. Scholl[2], I. Sheikh[1], K. Wang[1] and D.I. Wilson[1]

[1]Department of Chemical Engineering and Biotechnology, University of Cambridge, New Museums Site, Pembroke Street, Cambridge CB2 3RA, UK

[2]Institute for Chemical and Thermal Process Engineering, Technische Universität Braunschweig, Langer Kamp 7, 38106 Braunschweig, Germany

[3]Department of Chemical Engineering, University of Bath, Building 9 West, Claverton Down, Cambridge CB2 3RA, UK

Submitted to

Experimental Thermal & Fluid Science

Revision 1

November 2010

Corresponding author

Dr YMJ Chew

Department of Chemical Engineering
University of Bath
Building 9 West
Claverton Down
Bath
BA2 7AY

e-mail jc604@bath.ac.uk

Application of fluid dynamic gauging to annular test apparatuses for studying fouling and cleaning

T. Gu[1], F. Albert[2], W. Augustin[2], Y.M.J. Chew[3,*], M. Mayer[2], W.R. Paterson[1], S. Scholl[2], I. Sheikh[1], K. Wang[1] and D.I. Wilson[1]

[1]Department of Chemical Engineering and Biotechnology, University of Cambridge, New Museums Site, Pembroke Street, Cambridge CB2 3RA, UK

[2]Institute for Chemical and Thermal Process Engineering, Technische Universität Braunschweig, Langer Kamp 7, 38106 Braunschweig, Germany

[3]Department of Chemical Engineering, University of Bath, Building 9 West, Claverton Down, Cambridge CB2 3RA, UK

ABSTRACT

Fluid dynamic gauging (FDG) is a non-contact technique for measuring the thickness and strength of fouling layers immersed in liquid *in situ*. Its application to an annular geometry across a range of possible flow conditions, from stagnant to turbulent flow regimes (annulus Reynolds number ~ 29 000), is demonstrated. Two modes of measurement are demonstrated: in the first, the pressure drop across the nozzle is fixed and the mass flow rate of liquid withdrawn through the gauge is measured. In the second, the mass flow rate of liquid is fixed and the pressure drop measured: the latter is a new mode of measurement and it is shown to perform equally well, with advantages for particular applications. The results were not affected significantly by the surface under study being heated, indicating that the technique is suitable for measuring deposit thicknesses *in situ* during fouling and cleaning experiments in annular devices which are commonly used in deposition studies. Computational fluid dynamics (CFD) simulations, which afford detailed information about the flow patterns and shear stresses imposed on the surface, showed good agreement with experimental data for tests in the laminar regime: simulation of the transitional and turbulent regimes was not attempted. A short study of whey protein fouling recorded mixed success owing to the softness of the deposit, but demonstrated the scope for FDG to monitor the development of fouling layers in these geometries.

Keywords: CFD, cleaning, deposit, fouling, strength, thickness.

INTRODUCTION

Fouling in heat transfer systems is often unavoidable and reduces energy efficiency and plant operability. Mitigation of fouling, and effective cleaning strategies, both require understanding of the mechanisms involved in deposition and cleaning. Experimental studies are often required to develop this knowledge. One of the key properties affecting cleaning and removal is the thickness and strength of a fouling deposit, which will change over time and is often difficult to quantify. Fouling layers formed in liquid systems are frequently problematic because the material contains a sizeable fraction of liquid and is therefore soft, transparent, or has similar properties to the liquid.

Tuladhar *et al*. [1] developed the technique of fluid dynamic gauging (FDG) for measuring the thickness of fouling deposits immersed in a liquid environment *in situ* and without contacting the layer. A schematic of the gauge is presented in Fig. 1, where the surface being studied is curved. The gauge works as a siphon, whereby a pressure difference between the fluid near the substrate surface and the discharge end of the gauge causes liquid to flow into the nozzle. This discharge flow rate, m, is measured and the pressure difference calculated. For a given pressure driving force the flow rate is uniquely related to the distance between the nozzle and the surface, *i.e.* the clearance, h. Measurements of m allow h to be calculated, and changes in h can be related to the increase (fouling) or decrease (cleaning) of deposit thickness. The main limitation is that the foulant should be sufficiently stiff that it does not change shape during the measurement. The gauge is operated so that its internal flow is always in the laminar regime.

The performance of the nozzle can be quantified using the nozzle discharge coefficient, C_d, which accounts for the energy losses due to the flow around the nozzle entrance. C_d is defined as the ratio of the actual to ideal mass flow rate through the nozzle:

$$C_d = \frac{m_{actual}}{m_{ideal}} = \frac{m}{\frac{\pi d_t^2}{4}\sqrt{2\rho\Delta p_{13}}} \quad (1)$$

where subscripts 1 and 3 refer to locations shown in Figure 1, d_t is the nozzle diameter and ρ the liquid density. The relationship between C_d and h/d_t should be independent of measurement mode. Prior to this work, workers have reported data where m was the measured variable (*i.e*. the suction driving force was maintained constant, here termed 'fixed suction'). An alternative mode of measurement is where the mass flow rate is maintained at a set level and the pressure drop across the nozzle measured, which we term 'fixed gauging flow'. We report results here demonstrating the concept of fixed gauging flow mode, which is useful for applications where the amount of liquid withdrawn from the bulk system needs to be controlled. In this mode the absolute pressure in the system can be adjusted as desired, which has particular advantages for measurements at high pressure: the gauging flow rate can be controlled by a valve and the pressure drop across the nozzle measured using a differential pressure sensor.

Tuladhar *et al.* [1] developed the technique of 'quasi-static FDG' to study surface layers on flat surfaces, where the bulk liquid was still, apart from the flow generated by the gauging action. This FDG variant has been successfully applied to fouling and cleaning studies on a diverse range of foulant materials and surfaces (reviewed by Saikhwan *et al*. [2]). They (Tuladhar *et al*. [3]) and later Hooper *et al*. [4] demonstrated that FDG can be applied to monitor deposit thickness during the growth and removal of whey protein layers on a flat surface exposed to a imposed bulk flow of liquid in a duct of square cross section (termed 'flow FDG') with a precision of ± 10 μm. Recently, Gu *et al*. [5] described the application of dynamic gauging to an inner convex surface of an annular duct. They reported results for quasi-static conditions and where the flow in the annulus was in the turbulent regime. This study extends that work to the laminar and transitional annular flow regimes, using both fixed suction and fixed gauging flow modes.

This paper presents experimental FDG results from two concentric *annular* devices, this geometry being a popular configuration for heat transfer and fouling experiments (*e.g*. the HTRI fouling probe [6]). The aim was to incorporate an FDG probe into annular systems to extend the types of data which can be generated in such investigations. The first device, at Cambridge (labelled apparatus 1, shown in Figure 2), was geometrically similar to an annular test cell under construction at Imperial College London for tests on crude oil fouling, with outer and inner annulus diameters of 35 mm and 21 mm, respectively [7]. Experiments were conducted in laminar, transitional and turbulent flows (corresponding to annulus Reynolds numbers in the range $90 < Re_{\text{annulus}} < 29\ 000$) and in quasi-static flow (no bulk flow in the annulus). The second device, labelled apparatus 2, located at Braunschweig, features outer and inner annular diameters of 30 mm and 12 mm (Figure 3), respectively. A detailed description of this apparatus is given in [8]: this device is similar to the HTRI fouling probe. The inner rod contained an electrical cartridge heater and was used for studies of dynamic gauging on a heated surface, as would arise in fouling tests.

Dynamic gauging measurements change the flow pattern near the surface being studied for the duration of the test, creating an additional contribution to the shear stress imposed on the surface to that imposed by the bulk flow. Knowledge of the magnitude of this contribution is important, particularly where gauging measurements are able to disturb the deposit. Gu *et al*. [5] reported computational fluid dynamics (CFD) simulations of the velocity fields and the shear stress acting on surface by the action of the gauging flow. The governing Navier-Stokes and continuity equations of the steady-state, laminar, Newtonian and incompressible flow were solved numerically using the finite element method (FEM), and the results gave good agreement with the experimental data. These simulations were extended in the current paper to include the presence of a heated surface, which affects the flow via the temperature sensitivity of the liquid viscosity. Simulations of the transitional and turbulent regimes were not attempted as these present considerable computational challenges in, for instance, the onset of instability in the convergent-divergent region at the nozzle and the selection of a turbulence model in these boundary-dominated flows.

A brief study of whey protein fouling on a heated surface using apparatus 2 is reported to demonstrate the application of FDG to study fouling buildup on annular probes. The whey protein solutions used were opaque so visual methods could not be used to monitor the growth of deposit without interrupting the test. The measurement mode was not optimized and lessons were learned for future, systematic studies of such materials.

APPARATUS

Apparatus 1

Apparatus 1 (Figure 2) was employed for the quasi-static, laminar, transitional and turbulent flow tests using water at 20 °C as the test fluid. The outer tube (i.d. 35.1 mm) was constructed from acrylic for visualisation purposes, while a length of 316 stainless steel rod was used for the inner tube (o.d. 21.3 mm). The length of the annulus is 1 m. The concentric annulus was held vertical. The outer tube was constructed from acrylic for visualisation purposes, while a length of 316 stainless steel rod was used for the inner tube, to ensure a stiff surface. Early trials using an acrylic inner tube experienced significant vibration which impaired the measurements. Concentricity was maintained using sets of three metal locating pins at the inlet and outlet of the annulus. To ensure fully developed flow the gauge is located 750 mm from the entry ($54D_h$). Water is pumped from a holding tank and passes upwards through the annulus. Three different flowmeters, labelled R1, R2 and R3, were used for measuring flow rates corresponding to the laminar, transitional and turbulent flow regimes, respectively. The mean velocity in the annulus for each case was: R1, 0.0068 - 0.055 m/s ($90 < Re_{annulus} < 800$); R2, 0.04 - 0.15 m/s ($600 < Re_{annulus} < 2100$); and R3, 0.26 - 2.06 m/s ($3\,580 < Re_{annulus} < 29\,000$), where $Re_{annulus}$ was defined in terms of D_h.

The gauge was operated with the bulk flow rate through the annulus maintained constant. In the ‘fixed suction’ operating mode, which applied to most of the results reported here, two pressures were responsible for driving the gauging flow. The first is the suction pressure caused by the hydrostatic head, H, which was maintained constant at 405 mm (equivalent to 3970 Pa). The second is the static gauge pressure, p_s, associated with the annular flow. This latter pressure was measured using a pressure sensor (KH-68110-10, Ashcroft; accuracy ± 34 Pa), located 750 mm from the inlet of the annulus, diametrically opposite the gauging nozzle. The measured p_s values ranged from −1100 Pa (at $Re_{annulus} = 90$) to 34 300 Pa (at $Re_{annulus} = 29\,000$).

In the ‘fixed gauging flow’ operating mode, the apparatus was modified to include a control valve on the outlet from the gauge, so that the gauging flow could be

controlled. A differential pressure transducer was connected between the static gauge pressure tapping and a point just upstream of the control valve, as shown in Figure 2.

Apparatus 2

Apparatus 2, shown in Figure 3, was used to study the behaviour of the gauge in a slightly different annular geometry (i.d. 12 mm, o.d. 30 mm), and where the inner surface was heated. This apparatus had been constructed as a fouling test unit (see [8]) and features a heated section similar to the HTRI fouling probe. The dynamic gauging sensor was retrofitted to the apparatus by changing the outer tube section. The inner rod was 430 mm long, with the heated section extending 406 mm from the end. The surface area of the heated section is 0.015 m^2. The inner heating rod surface material was 316 stainless steel, while the outer pipe was acrylic. The annulus was again located vertical with liquid flowing upwards. The temperature of the rod, T_w, is measured at a location close to, but beneath, the rod surface. Heat flux, q, is measured from the preset power input (7 - 25 kW/m^2). The bulk liquid temperature, T_{bulk}, was measured by thermocouples located at the inlet and outlet temperature of the test section, and the inlet temperature was maintained constant over time using a plate heat exchanger operating as a cooler with cold water as the utility. Liquid was circulated through the test section by the centrifugal pump, with automated control of the bypass value maintaining a steady flow rate.

This apparatus was used for a short feasibility study using dynamic gauging, in the fixed pressure mode, to monitor whey protein fouling. Whey protein concentrate powder (ULTRALAC 35LH) was supplied by Biolac, Germany, with manufacturer's composition description: protein, 35 ± 2 wt%; lactose (monohydrate), 45 ± 2 wt%; fat, max. 4 wt%; ash, max. 8 wt%; humidity, max. 5 wt%. The solution was prepared by adding a set mass of WPC powder (1.67 kg) to de-ionised water (10 L) at 50 °C in a container. The solution was agitated by an overhead stirrer until all visible lumps disappeared, yielding a cloudy solution. In the fouling experiments the bulk temperature of the WPC solution was maintained at 54 °C. The pH was set constant at pH 6 by addition of dilute hydrochloric acid (0.1 M). Fouling experiments were performed at two different inner rod temperatures.

The gauge was calibrated with de-ionised water before the start of each fouling experiment. Once calibration of the gauge was complete, electrical power was applied to the inner rod to achieve an initial measured wall temperature of 95 °C (experiment 1) or 106 °C (experiment 2). As the fouling layer builds up, the wall temperature (T_w) increases; the increase in T_w was logged on a PC alongside other temperatures, heat flux, pressure and flow rate at 5 min intervals. The mass flow rate through the annulus was maintained constant over the course of each experiment. The apparatus was allowed to run overnight to build up a fouling layer.

Gauging nozzles

Both gauges were fabricated from 316 stainless steel with dimensions d_t = 1 mm, d = 4 mm and λ = 1.5 mm (Figure 1), but with slightly different shapes: the gauge in apparatus 1 had dimensions k = 2 mm, s = 0.5 mm and α = 45°, while that in apparatus 2 had k = 1 mm, s = 0.12 mm and α = 30°.

Both gauges were moved backwards and forwards horizontally, normal to the inner tube, through a seal using a micrometer. These operating modes are referred to as *nozzle retreating* and *nozzle advancing*, respectively. The micrometer read the distance between the surface of the inner rod and the tip of the nozzle, h. The discharge gauging flow was measured using an electronic balance (accuracy ± 0.05 g).

The gauging nozzle was connected to a tube of true length, l = 525 mm (apparatus 1) and l = 393 mm (apparatus 2), with the other end open to the atmosphere. The value of the tube effective length, l_{eff}, used to account for frictional losses along the tube, fittings and in the bend, varied with the tube Reynolds number. The value of l_{eff} was determined by separate experiments employing a reservoir of stagnant liquid and with the nozzle removed from the end of the tube, performed at clearances greater than 20 mm (h/d_t » 2). The frictional loss along the siphon tube, Δp_{34}, was then balanced by the hydrostatic head driving the flow. The value of l_{eff} at different tube Reynolds numbers was determined using the Hagen-Poiseuille relationship. The effective length, l_{eff}, was finally used to calculate Δp_{34} for evaluation of Δp_{13} in equation (1) [1].

NUMERICAL SIMULATIONS

CFD simulation was employed to model the flow patterns arising in annular flow FDG measurements in the laminar regime ($Re_{annulus} \leq 560$). Simulations of the flows in quasi-static FDG in annular geometries were reported in [5] and those for laminar bulk flows along rectangular ducts were reported in [11 - *NB need to change reference numbers*]. The simulations reported here combine these earlier models. Two 3-dimensional models are presented: the model for apparatus 1 involved only fluid flow, while the model for apparatus 2 involved both fluid flow and heat transfer. The liquid in both cases was water. The CFD computations were performed using the commercial FEM software, COMSOL MULTIPHYSICS^{TM} (version 3.5, Chemical Engineering Module). All flows were assumed to be laminar and at steady state. The continuity and Navier-Stokes equations for a Newtonian liquid are:

Continuity: $$\nabla \cdot \mathbf{v} = 0 \quad (2)$$

Navier-Stokes: $$\rho \mathbf{v} \cdot \nabla \mathbf{v} = -\nabla p + \mu \nabla^2 \mathbf{v} + \rho \mathbf{g} \quad (3)$$

where $\mathbf{v}$ is the velocity vector, p the pressure, ρ the density, μ the dynamic viscosity and g the acceleration due to gravity, set to zero in this case for computational convenience [9]. Density and viscosity values were assumed to be at 20 ^{o}C and set constant throughout the system for apparatus 1.

The steady state energy equation can be written as:

$$\rho C_p \left(\mathbf{v} \cdot \nabla T \right) = \nabla \left(\beta \nabla T \right) + Q_s \quad (4)$$

where C_p is the specific heat capacity, T is the temperature, β is the thermal conductivity and Q_s is the heat sink/source. As the temperature changes, the physical properties of the fluid are no longer constant. Instead ρ, μ, C_p and β are functions of the temperature. There is an option in the software which allows these properties to be

selected (as a function of temperature); this was applied in the heat transfer model *i.e.* apparatus 2.

Boundary conditions (momentum transfer)

A three-dimensional model was set up illustrating a quarter of the annulus and half of the gauge, exploiting symmetry along the *y*-*z* plane for the tube and both the *x*-*z* and *y*-*z* planes for the annulus (Figure 4). The length of the annulus and the tube were shortened to reduce computing time. The liquid enters the system through the annulus base and leaves through the gauging tube and through the annulus top. The imposed boundary conditions were:

(i) Annulus base ($z = 0$)

Fully developed laminar flow was assumed, so that the *z*-wise velocity (w) was approximated by [10],

$$w_{annulus} = \frac{2m_{annulus}}{\pi\rho}\left\{1-\left(\frac{y}{D_o/2}\right)^2 - \frac{1-\kappa^2}{\ln\left(1/\kappa\right)}\ln\left(\frac{D_o/2}{y}\right)\right\} \div \left\{(1-\kappa^4) - \frac{(1-\kappa^2)^2}{\ln\left(1/\kappa\right)}\right\} \quad (5)$$

where $m_{annulus}$ is the mass flow rate through the annulus, taken from experiment, and κ is the ratio between the inner and outer radii of the annulus.

The *x*-wise and *y*-wise velocities u and v were set to zero at this plane.

(ii) Annulus top, $z = L'$

The annulus length to diameter ratio, L'/D_h, was 7.5, determined via trial and error to be sufficient for the streamlines to be parallel at the top of the annulus. The pressure at the top is set to the (negative) gauge pressure, p_s, measured in experiment.

$$p_1' = -p_s \quad (6)$$

(iii) Gauging tube outlet, $y = l'$

Fully developed flow is established, following the Hagen-Poiseuille velocity profile, *viz*.

$$v = v_{\max}\left(1-\left(\frac{2r}{d}\right)^2\right) \quad (7)$$

where r is the radial coordinate measured from the tube centre-line and $v_{\max}$ is the maximum y-wise velocity, being twice the mean velocity calculated from experimental data. The x-wise and z-wise velocities u and w are set to zero. The length of the tube used in the simulations was $l'/d = 45$, obtained by a numerical trial and error search for fully developed flow at the tube outlet.

(iv) Walls

The walls of the annulus, gauge, nozzle and the lip of the nozzle are all modelled as impermeable with no slip.

(v) Symmetry

There is no flow across the y-z and x-z planes of symmetry, thus $\mathbf{n}\cdot\mathbf{v} = 0$, where $\mathbf{n}$ is the normal vector of the relevant plane.

Boundary conditions (energy transfer)

Experiments on heated surfaces were performed using apparatus 2. The geometry of the CFD model was similar to the one described above. In addition to the boundaries specified for the continuity and the incompressible Navier-Stokes equations, the following boundaries were specified in the heat transfer model.

(i) Annulus base, $z = 0$

Uniform inlet temperature was imposed at the annulus base. The value was taken from measurement of the bulk temperature from the experiment, measured at the inlet of the test section.

$$T = T_o \quad (8)$$

(ii) Annulus inner tube

Uniform temperature was imposed at the surface of the inner tube. The value was taken from measurement of wall temperature from the experiments (Figure 3). The wall temperature did not vary much, *i.e.* ± 1 °C, over the course of the gauging calibration experiments while the flow rate was maintained constant. Uniform temperature was therefore considered a reasonable assumption in simplifying the model. For the cases presented here, the temperature at the inner surface of the annulus was specified at T_w = 20 °C, 50 °C or 80 °C.

(iii) Annulus top, z = L'

Heat transfer by convection was specified at the top of the annulus. This assumes that all energy passing through this boundary did so through convective heat transfer, *i.e.* heat is transported by fluid motion. This boundary condition is used in convection-dominated energy balances where the outlet temperature was unknown (COMSOL, Chemical Engineering Module).

(*iv*) *Walls*, *Symmetry and Gauging tube outlet*, *y = l'*

No heat flowed across the rest of the boundaries in the model domain, which included the walls of the gauge and the annulus, the *y-z* plane of symmetry and the gauging tube outlet. Therefore, the boundary specified the heat flux to be zero, *viz.*

$$\mathbf{n} \cdot \mathbf{q} = 0 \quad (9)$$

where **q** is the heat flux vector and **n** is the normal vector of the relevant surface.

Mesh

The simulation domain was meshed with tetrahedral elements using the software's built-in mesh-generator. A higher concentration of computational elements was

assigned to the clearance region beneath the nozzle. This is the region with the steepest velocity and pressure gradients, so the mesh was refined in order to obtain satisfactory resolution there. The size of the elements at the nozzle region was set approximately ten times smaller than the elements in the rest of the domain. The number of elements, N_e, varied with h/d_t, l'/d, L'/D, $Re_{annulus}$ and Re_{tube}. In this work, N_e varied between 2 000 and 25 000. Further details of the simulation configuration are given in [5].

To verify the accuracy of a particular solution, the number of elements (N_e) was varied, as summarized in Table 1. Better agreement between the experimental and simulation C_d values was obtained with more elements, as expected, with the associated increase in computational time. Solutions took between 5 to 180 min, using a desktop PC with a 2.61 GHz dual core processor and 3.25 GB RAM. Convergence was tested by comparing the values of velocity and pressure from successive iterations; tolerances were set at 10^{-6} m/s (*cf.* a lowest radial mean velocity in the gauging tube of 3×10^{-3} m/s) or 10^{-6} Pa (*cf.* a lowest reference pressure of 860 Pa), for the velocity and pressure, respectively. The tolerance dictates the error in each integration step.

Another indication of numerical accuracy is given by testing the conservation of mass. Mass balance calculations yielded agreement to 10^{-5} kg/s or better for all cases investigated. This value was obtained by subtracting the annulus base (inlet) flow rate from the sum of the gauging tube and annulus top (both outlet) mass flow rates. In comparison, the smallest gauging tube mass flow rate was 4.8×10^{-4} kg/s.

RESULTS AND DISCUSSION

Calibration

Figure 5(a) shows a series of mass flow rate – clearance profiles for apparatus 1, spanning the range $90 \leq Re_{annulus} \leq 29\ 000$. The general increase in m with $Re_{annulus}$ is related to the increase in p_s with bulk flow rate. It is worth mentioning that when there is no annular flow, the pressure gauge records a negative value of p_s. This is because of the location (hence the liquid level) of the supply tank. At low $Re_{annulus}$, the static pressure due to bulk annular flow is low, thus, the pressure gauge records a negative value. For laminar annular flows, the working range for the gauge, *i.e.* where m is sensitive to h/d_t, lay between 0.06 to 0.30. It can be seen that as $Re_{annulus}$ increases, the working range extends to $h/d_t = 0.4$ for $Re_{annulus} = 29\ 000$. These results are consistent with those of Gu *et al.* [5], where three zones of interest were identified, namely (*i*) *curvature*, (*ii*) *incremental* and (*iii*) *asymptotic*. In the latter region the flow rate, labeled m_∞, is insensitive to h/d_t and is therefore not useful for gauging. This is also the case with the *curvature* zone, which arises from the presence of a curved surface. This can be clearly observed in Figure 5(a), where m does not reach zero because there is always a gap between the flat nozzle tip and the curved substrate surface for liquid to flow through. The incremental region is the one exploited in gauging measurements.

Figure 5(b) shows that the same trends in mass flow rate – clearance profiles were observed with apparatus 2 and the 30° nozzle, for $Re_{annulus}$ values ranging from 250 to 10 000. The working range of apparatus 2 lay between $0.02 \leq h/d_t \leq 0.3$. However, the curvature zone was smaller. This difference is attributed to the differences in the apparatus geometry. The diameter of the inner rod on apparatus 1 is almost twice that of apparatus 2 (21 mm *cf.* 12 mm), whilst the nozzle throat sizes are identical ($d_t = 1$ mm). This means that with respect to the liquid near the nozzle throat, the geometry of apparatus 1 is closer to that of a parallel plate when the nozzle is very close to the surface ($h/d_t < 0.04$). For apparatus 2, for a given clearance the surface curvature is larger, allowing more liquid to flow and thereby reducing the extent of the curvature zone.

The difference between the two apparatuses and the two nozzles are compared in Figure 5(c), which shows the data in the form of discharge mass flow rate divided by m_∞ to yield a dimensionless profile. For the same clearance, more liquid flowed through gauge 2, due to a higher pressure driving force, a smaller nozzle rim, and a larger hydraulic diameter. The change in the nozzle geometry will also affect the mass flow rate, and this needs to be investigated separately. The Figure shows that the working range of the gauge for both nozzles lies in the range $0.06 < h/d_t < 0.30$.

For virtually all cases reported above, m_∞ was ≤ 15% of the total flow through the annulus. For the $Re_{annulus} = 90$ (apparatus 1) case m_∞ approached 30% of the flow through the annulus inlet. This is unlikely to be desirable in a monitoring experiment, both because of the impact on flow downstream and also because hysteresis effects have been observed at these high flow fractions [3].

Discharge coefficient

The effect of the geometry on the nozzle performance can be quantified via C_d. In the 'fixed suction' operating mode the C_d-h/d_t profiles mirror the m-h/d_t profiles in Figure 5 as m_{ideal} is constant. The effect of nozzle geometry on the asymptotic nozzle discharge coefficient, $C_{d,\infty}$, defined here as the average value of C_d at large clearances (*e.g.* $h/d_t \geq 0.6$), is shown in Figure 6 for different values of $Re_{annulus}$. The 45° and 30° nozzles behaved quite differently; $C_{d,\infty}$ decreased gradually with $Re_{annulus}$ for the 45° nozzle (apparatus 1), suggesting that the nozzle behaves more ideally at lower annular flows, whereas for the 30° nozzle the opposite trend was observed. The latter has a smaller angle which is likely to reduce the amount of recirculation within the nozzle. Also, the nozzle rim was narrower which reduces the frictional losses underneath the rim. Both of these factors contribute to lowering the hydraulic losses across the nozzle, which increase the value of C_d. For the lowest $Re_{annulus}$ values investigated, *i.e.* 90 and 250 for the 30° and 45° nozzle, respectively, both nozzles gave a common C_d value of around 0.68.

In the 'fixed gauging flow' operating mode, the mass flow rate is maintained relatively constant and the pressure drop across the nozzle is the measured variable. Figure 7(*a*) shows two pressure drop-h/d_t profiles obtained for similar bulk and gauge

flow rates, and different total pressure in the duct. The data show very good agreement, within the bounds of experimental error. Data are not reported for h/d_t < 0.1 as the pressure drop exceeded the range of the differential pressure transducer used. The associated C_d-h/d_t profiles are presented in Figure 7(b), alongside sets obtained using the fixed suction operating mode at similar annulus flow rates. The agreement between the two modes is excellent and indicates that either mode can be used for deposit thickness measurement. The advantage of the fixed gauging flow mode is that the amount of liquid withdrawn from the bulk flow (and thus the impact of the measurement on the bulk flow characteristics) is controlled. Fixing m also affects the shear stress imposed on the surface, and could be used to set a maximum shear stress for the measurement. This mode does, however, require an accurate differential pressure cell which may not always be available.

Heated surfaces

The presence of a heated surface was studied using apparatus 2 in the 'fixed suction' operating mode. Figure 8 shows that there was little effect of surface temperature on the discharge mass profiles over the range of heat fluxes and flow rates tested. The wall temperatures were maintained at 20 °C, 50 °C, 80 °C and 110 °C for $Re_{annulus}$ values of 1700, 3000 and 10 000, representing flows in the laminar, transitional and turbulent regime. The corresponding heat fluxes lay in the range 7 - 25 kW/m^2.

A slight increase in mass flow rate (6% or less) was noticed for the higher wall temperatures when the nozzle was located near the heated surface. This was attributed to the lower viscosity of the liquid in this region. Little difference was observed beyond 220 μm from the heated surface (h/d_t = 0.22). These results indicate that FDG can be used to study fouling in these annular geometries. A noteworthy feature is that these experiments were occasionally affected by bubble formation promoted by the hot surface, which affects the performance of the gauge.

CFD simulation

Table 2 summarises the results for a series of CFD simulations of FDG experiments performed in (laminar) annular flow on apparatus 1. The experimental and computed values of C_d agreed to 10% or better for all cases. The simulated C_d values lie for

most cases within, or close to, the experimental C_d error bars. For the range of $Re_{annulus}$ investigated, the agreement appears better for the lower $Re_{annulus}$ flows and for larger clearances ($h/d_t > 0.10$).

The associated flow velocity distributions in the tube (y-direction) are presented in Figure 9. The highest velocity occurs within the throat of the nozzle with expansion further along the tube. Asymmetrical flow in the tube is noticed when the gauge is close to the surface, at $h/d_t = 0.10$, where the momentum from the annular flow is more influential, in agreement with results for square ducts reported by Gu *et al.* [11]. The flow in the nozzle and tube becomes more symmetrical when the gauge is further away from the surface, *e.g.* $h/d_t \geq 0.14$.

Values of shear stresses acting on the surface being gauged could be extracted from the CFD simulations. The surface is curved and hence the stresses acting on the surface along the annulus in the z-direction, and across the annulus in the x-direction, are different. Shear stress values are presented in Figure 10(*a*) along the inner surface of the annulus in the z-direction, and in Figure 10(*b*) along the arc length of the inner surface in the x-direction, for the simulation case $h/d_t = 0.10$ and 0.20, for $Re_{annnulus}$ 560 and 90, respectively. The z-wise shear stress ($\tau_{yz'}$) is approximately zero at the centerline of the tube ($z' = 0$), reaches a maximum beneath the nozzle lip ($z' = 0.5$ to 1.0 mm) and approaches zero asymptotically for $z' > 1$ mm. The magnitude of the z-wise shear stress at a given value of z' decreases as the gauge is further away from the surface. The magnitude of these shear stresses is comparable with velocities used in cleaning-in-place operations [12].

As the flow rate through the annulus increases, so does the shear stress on the surface underneath the gauging nozzle, but the dominant shear stress is that caused by the proximity of the gauge to the surface. When the gauge is close to the surface, *i.e.* at $h/d_t = 0.10$, the shear stress is slightly higher upstream of the gauge, which is an effect of the flow in the annulus.

The gap between the nozzle and the surface increases along the arc (Figure 10(*b*)). The highest values of shear stress (τ_{za}) occur within the throat and underneath the

nozzle rim. The magnitude and shape of τ_{za} are similar to τ_{yz}, when the gauge is close to the surface, for h/d_t of 0.10 and 0.14. However, when the nozzle is further away, at a clearance of h/d_t = 0.20, the shear stress τ_{za} exerted on a curved surface by the nozzle is less pronounced, and the shear stress decays steadily from the centreline of the tube, rather than displaying peaks underneath the nozzle rim.

Figure 11 shows the effect of the wall surface temperature on the shear stress (for apparatus 2). The values of shear stress are different for different wall surface temperature. There is a clear decline in the peak shear stress as the temperature of the surface increases from 20 °C to 50 °C and 80 °C. This could be explained by the fact that as the wall surface temperature increases, the fluid near the heated surface becomes less viscous. The fluid flows more readily, as a result the shear stress caused by the gauging flow decreases.

Whey protein fouling

5 wt% aqueous solutions of whey protein concentrate (WPC) was passed through apparatus 2 and allowed to run without interruption for 14 hr. The bulk temperature of the solution was maintained at 53 °C, the wall temperature at 95 °C, and a flow rate through the annulus of 0.22 m/s, corresponding to $Re_{annulus}$ = 7500. After 10 hr an increase in fouling resistance (R_f) was observed, shown in Figure 12, which indicated the formation of a fouling layer. The linear fouling rate was determined from the slope of R_f against time plot, as shown in Figure 12. The value obtained, of 1.5×10^{-4} $m^2K/W.hr$ (equivalent to 4×10^{-5} m^2 K/kJ), is similar to the initial fouling rates ~10^{-5} m^2 K/kJ reported by Rose for dilute WPC solutions [13].

FDG measurements were made using the fixed pressure mode after 2 hours. Apparatus 2 was not configured to operate in fixed gauging flow mode. The gauge measured a thickness of 220 μm. Due to resources and time limitations, no repeats were performed for these fouling experiments. Gu *et al.* [5] claimed the accuracy of the current FDG configuration to be ± 10 μm. The protein layer was soft and gel-like, and the photographs in Figure 13 indicate that the deposit was removed from the surface by the gauging flow. Lumps of the deposit were observed in the discharge flow from the tube during the gauging experiment when the nozzle was close to the

deposit surface. This is undesirable for the purpose of thickness measurement but will be useful for deposit strength measurement (not presented in this work). Therefore, the authors expect the error in the thickness values is more than ± 10 μm. More experiments would be needed to quantify the value. The removal behaviour was observed in repeated trails and indicated that lower gauging flow rates should be used with these deposits: fixed gauging flow mode would also be preferable. The layer dried quickly once the system had been drained. The nozzle left a ring of diameter 2 mm, in good agreement with the CFD predictions, suggesting that the dominant removal mechanism was related to adhesive failure.

The observation of deposit being removed in lumps raises the prospect of nozzle blockage. In practice this is monitored by withdrawing the gauge away from the surface between measurements and recording m_∞ (in constant pressure mode) or ΔP_∞ (with constant gauging flow). Nozzle blockage would cause deviations from the values recorded during the initial calibration, and could be corrected by stopping and/or reversing the gauging flow.

The thermal conductivity of the WPC fouling layer, β_d, can be estimated knowing the deposit thickness

$$\beta_d = \frac{\delta}{R_f} = \frac{220\times10^{-6} \pm 27.8\%}{0.91\times10^{-3} \pm 0.05\%} \approx 0.24 \pm 0.08 \text{ W/m K} \quad (10)$$

The estimated value of 0.24 W/m K is similar to values reported in previous work ([4] and [14]), and lie within the range of those reported.

These initial studies using an annular fouling probe indicated that FDG can be used to study fouling build-up but highlights. The technique requires careful method development when soft deposits are being studied.

CONCLUSIONS

This work has demonstrated that fluid dynamic gauging can be used, in principle, for measuring the thickness of layers on the inner surface of an annular duct in the presence of a flowing liquid where the bulk flow is in the laminar, transitional or turbulent regime. Similar calibration characteristics were obtained for two different annular geometries, both of which are relevant to studies of fouling and cleaning. A new mode of gauging measurement, where the gauging flow was fixed and the pressure drop across the nozzle measured, was introduced. Calibrations obtained for a heated surface, at various wall temperatures, confirmed that FDG can be used with a heated surface as employed in fouling test systems. The practical working range of the gauge proved to be independent of the surface being heated. CFD simulations of flow patterns were performed for cases where the bulk flow was in the laminar regime and gave good agreement with experimental results.

The heated annulus apparatus was used in a short study of fouling by whey protein solutions. The deposit generated was soft and could be removed by the gauging flow, indicating that the gauging conditions required optimization. The deposit removal patterns were consistent with the CFD simulation results, which indicated that the highest shear stresses are located under the rim of the gauging nozzle.

ACKNOWLEDGEMENTS

Funding for the Cambridge work from EPSRC (EP/D50306X), and a Research Fellowship for YMJC from the Royal Academy of Engineering, are gratefully acknowledged. This international collaboration was funded by the British Council and DAAD. The FDG apparatuses were constructed by Gary Chapman (Cambridge) and Karl Karrenführer (TU-BS).

NOMENCLATURE

a arc length along annulus cross section, m

C_d discharge coefficient, dimensionless

C_p specific heat capacity, J/kgK

d inner diameter of dynamic gauging tube, m

d_t nozzle throat diameter, m

D_h hydraulic diameter of the annulus, m

D_o outer diameter of the annulus, m

g acceleration due to gravity, m/s^2

h clearance between nozzle tip and gauging surface, m

H hydrostatic head providing pressure driving force for gauging flow, m

k wall thickness of gauging tube, m

L' CFD model duct length, m

l length of siphon tube, m

l' CFD model tube length, m

m tube discharge mass flow rate, kg/s

$\boldsymbol{n}$ normal vector

N number

p pressure, Pa

p_s static pressure, Pa

q heat flux, W/m^2

Q_s heat sink/source, W

r radial coordinate of the gauging nozzle, m

R_f fouling resistance, m^{2}K/W

Re Reynolds number, dimensionless

s width of nozzle rim, m

t time, s

T temperature, °C

u x-wise velocity, m/s

$\mathbf{v}$ velocity vector

v y-wise velocity, m/s

$\bar{v}$ mean y-wise velocity, m/s

w z-wise velocity, m/s

$\bar{w}$ mean z-wise velocity, m/s

x, y, z coordinates

Greek letters

α	nozzle inner angle, °
β	thermal conductivity, W/mK
δ	thickness of deposit, m
κ	ratio between inner and outer diameter of annulus
λ	length of nozzle exit, m
μ	dynamic viscosity, Pa.s
ρ	density, kg/m^3
$\tau_{yz'}$	shear stress on the *y*-plane in the *z*-direction, Pa
τ_{za}	shear stress on the *z*-plane in the *a*-direction, Pa

Subscript

actual	actual
annulus	annulus
bulk	bulk
d	deposit
e	elements
eff	effective
exp	experimental
ideal	ideal
max	max
sim	simulation
tube	tube
w	wall
∞	asymptotic

Acronyms

CFD	computational fluid dynamics
FDG	fluid dynamic gauging
FEM	finite element method
HTRI	Heat Transfer Research Incorporated
TU-BS	Technische Universität Braunschweig
WPC	whey protein concentrate

REFERENCES

[1] T.R. Tuladhar, N. Macleod, W.R. Paterson, D.I. Wilson, Development of a novel non-contact proximity gauge for thickness measurement of soft deposits and its application in fouling studies, Canadian Journal of Chemical Engineering, 78 (2000) 925-947.

[2] P. Saikhwan, Y.M.J. Chew, W.R. Paterson, D.I. Wilson, Fluid dynamic gauging: a technique for studying the cleaning of food process surfaces, Food Manufacturing Efficiency, 1(2) (2007) 34-41.

[3] T.R. Tuladhar, W.R. Paterson, D.I. Wilson, Dynamic gauging in duct flows, Canadian Journal of Chemical Engineering, 81 (2003) 279-284.

[4] R.J. Hooper, W. Liu, P.J. Fryer, W.R. Paterson, D.I. Wilson, Z. Zhang, Comparative studies of fluid dynamic gauging and a micromanipulation probe for strength measurements, Food & Bioproducts Processing, 84 (2006) 353-358.

[5] T. Gu, Y.M.J. Chew, W.R. Paterson, D.I. Wilson, Experimental and CFD studies of fluid dynamic gauging in annular flows, AIChE Journal, 55(8) (2009a) 1937-1947.

[6] C.A. Bennett, R.S. Kistler, K. Nangia, W. Al-Ghawas, N. Al-Hajji, A. Al-Jemaz, 2007, Observation of an isokinetic temperature and compensation effect for high temperature crude oil fouling, ECI conference on heat exchanger fouling and cleaning, Tomar, Portugal, Vol. RP5.

[7] S. Macchietto, G.F. Hewitt, F. Coletti, B.D. Crittenden, D.R. Dugwell, A. Galindo, G. Jackson, R. Kandiyoti, S.G. Kazarian, P.F. Luckham, O.K. Matar, M. Millan-Agorio, E.A. Müller, W. Paterson, S.J. Pugh, S.M. Richardson, D.I. Wilson, 2009, Fouling in Crude Oil Preheat Trains: a Systematic Solution to an Old Problem, EUROTHERM conference on Fouling and Cleaning in Heat Exchangers, Schladming, Austria.

[8] K. Bode, R.J. Hooper, W. Augustin, W.R. Paterson, D.I. Wilson, S. Scholl, Pulsed flow cleaning of whey protein fouling layers, Heat Transfer Engineering, 28 (2007) 202-209.

[9] D.J. Tritton, Physical Fluid Dynamics, second edition, Oxford University Press, UK, 1988.

[10] R. Bird, W.E. Stewart, E.N. Lightfoot, Transport Phenomena, second edition, John Wiley & Sons Inc., 2002.

[11] T. Gu, Y.M.J. Chew, W.R. Paterson, D.I. Wilson, Experimental and CFD studies of fluid dynamic gauging in duct flows, Chemical Engineering Science, 64(2) (2009b) 219-227.

[12] D.A. Timperley, Cleaning in place, Journal of Dairy Technology, 42(2) (1989) pp. 32-33.

[13] I.C. Rose, Model investigations of initial fouling rates of protein solutions in heat transfer equipments, PhD Dissertation, Department of Chemical and Bio-resource Engineering, University of British Columbia, 1999.

[14] T.R. Tuladhar, W.R. Paterson, D.I. Wilson, Thermal conductivity of whey protein undergoing swelling. Measurement by dynamic gauging, Food & Bioproducts Processing, 80 Part C (2002) 332-339.

List of table captions

Table 1: Mesh refinement result for the simulation case $h/d_t = 0.1$, $Re_{annulus} = 90$, $Re_{tube} = 150$.

Table 2: Summary of CFD simulation of FDG in annular flow (Apparatus 1), isothermal case.

List of figure captions

Figure 1: (*a*) Schematic and (*b*) photograph of fluid dynamic gauge (FDG) in an annular geometry (apparatus 1). The schematic shows dimensional parameters of the gauge. Numbers 1 to 4 signify various locations in the system.

Figure 2: Schematic of apparatus 1: A - annular test section; B - electronic balance; C - gauging flow control valve; DP - differential pressure cell; F - filter; G - gauging tube; *H* - hydrostatic head; M - micrometer; P - pressure sensor; R- flowmeter; V - bulk flow control valve.

Figure 3: Schematic of apparatus 2: A - annular test section; B - electronic balance; F – flow controller; FI - flow indicator; G - gauging tube; HX - heat exchanger; PI - pressure sensor, TI - temperature sensor.

Figure 4: Simulation geometry. Numbers refer to the stations in the simulation. The arrows indicate the entry flow in the annulus, and the exit flow in the tube and annulus top. Co-ordinates: *z* - vertical (annulus) axis; *y* - horizontal (gauging tube) axis. Velocity components *w* and *v* are indicated.

Figure 5: Effect of Re_{annulus} on experimental FDG mass profile. Regions marked: (*i*) *curvature* zone; (*ii*) *incremental* zone; (*iii*) *asymptotic* zone. (*a*) Apparatus 1, $\alpha = 45°$, $H = 405$ mm; (*b*) Apparatus 2, $\alpha = 30°$, $H = 350$ mm. (*c*) Data replotted as dimensionless mass flow rate – clearance profiles; solid symbols, Apparatus 1, open symbols Apparatus 2.

Figure 6: Effect of Re_{annulus} on asymptotic nozzle discharge coefficient $C_{\text{d},\infty}$ for gauge in apparatus 1 and 2, respectively. Solid circles: gauge 1; open circles: gauge 2.

Figure 7: Fixed gauging flow rate mode, apparatus 1: (*a*) effect of h/d_{t} on pressure drop across the gauging nozzle, $Re_{\text{annulus}} = 1100$, $m \sim 1.1$ g/s; (*b*) discharge

coefficient. Circles - p_s = 700 Pa, triangles - p_s = 2800 Pa, crosses - data set from fixed suction mode, $Re_{annulus}$ = 1100, p_s = 2600 Pa.

Figure 8: Effect of wall temperature on discharge mass flow rate. Apparatus 2, fixed suction operating mode. Bulk flow temperature, 20 °C, H = 350 mm. Symbols: squares - surface temperature = 20 °C; circles, 50 °C; triangles, 80 °C; crosses, 110 °C.

Figure 9: Simulated tube (y-wise) velocity component at the y-z plane of symmetry for apparatus 1, at $Re_{annulus}$ values of (*a*) 560 and (*b*) 90. The simulation shows that the maximum y-wise velocity occurs at the nozzle throat.

Figure 10: Shear stresses imposed by the gauging flow on the inner surface of the apparatus 1 annulus (*i.e.* at y = 0), directly underneath the gauge, as illustrated in the insets. (*a*) stress along the inner surface of the annulus in the z'-direction, $\tau_{yz'}$. (*b*) Shear stress, τ_{ya}, imposed by the gauging flow on the inner surface of the annulus at different positions along the arc, a.

Figure 11: Heated surface annular flow mode FDG (apparatus 2): Shear stress imposed by the gauging flow on the inner convex surface of the annulus (at y = 0), as a function of the annulus axial coordinate measured from the gauge central axis. Conditions: $Re_{annulus}$ = 1700, Re_{tube} = 500, p_s = −920 Pa, h/d_t = 0.18. Circles, 20 °C; triangles, 50 °C; squares, 80 °C.

Figure 12: Fouling in 3.5 wt% WPC solution using apparatus 2 (experiment 1). Experimental conditions: $Re_{annulus}$ = 7300, T_{bulk} = 53 °C, p_s = 7580 Pa, pH = 6. Symbols: unfilled - T_w; solid - R_f. Error bar is represented by the size of the symbols. Vertical dashed line at A marks the time at which FDG measurements were made. Solid locus - linear regression to initial growth data, giving R_f (in m^2K/W) = 1.5×10^{-4} t (in hr) – 1.02. R^2 = 0.95.

Figure 13: Images of the ring left by the gauging nozzle (*a*) *in-situ*, after fouling experiment 1; (*b*) *ex-situ*, using a digital microscope under 50× magnification.

(a)

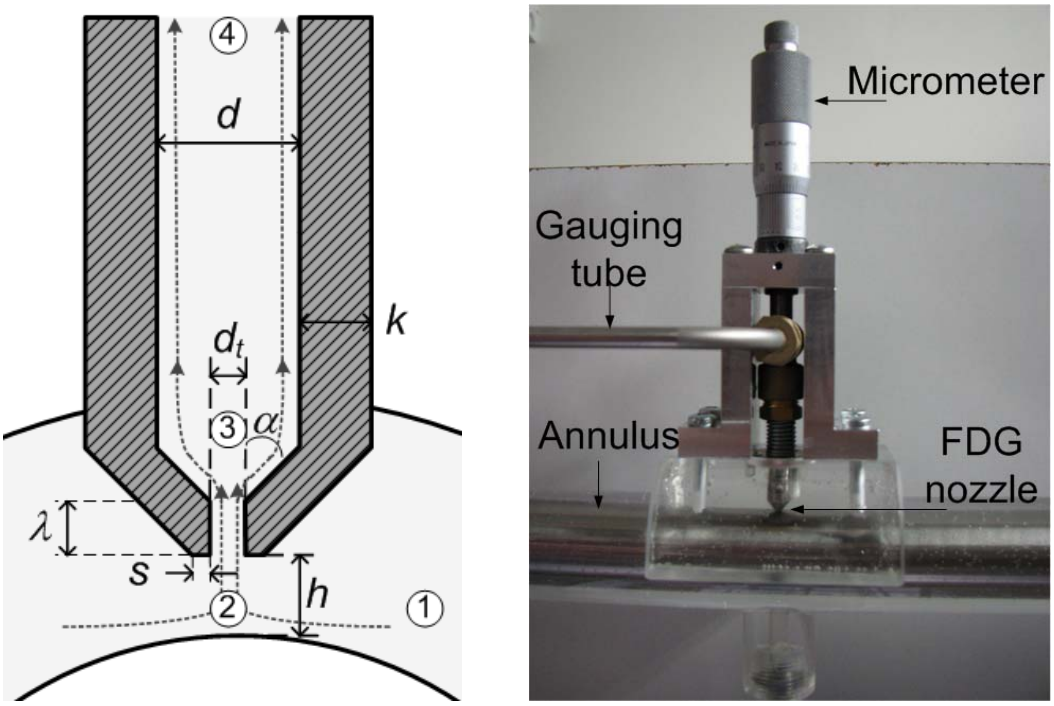

Figure 1: (*a*) Schematic and (*b*) photograph of fluid dynamic gauge (FDG) in an annular geometry (apparatus 1). The schematic shows dimensional parameters of the gauge. Numbers 1 to 4 signify various locations in the system.

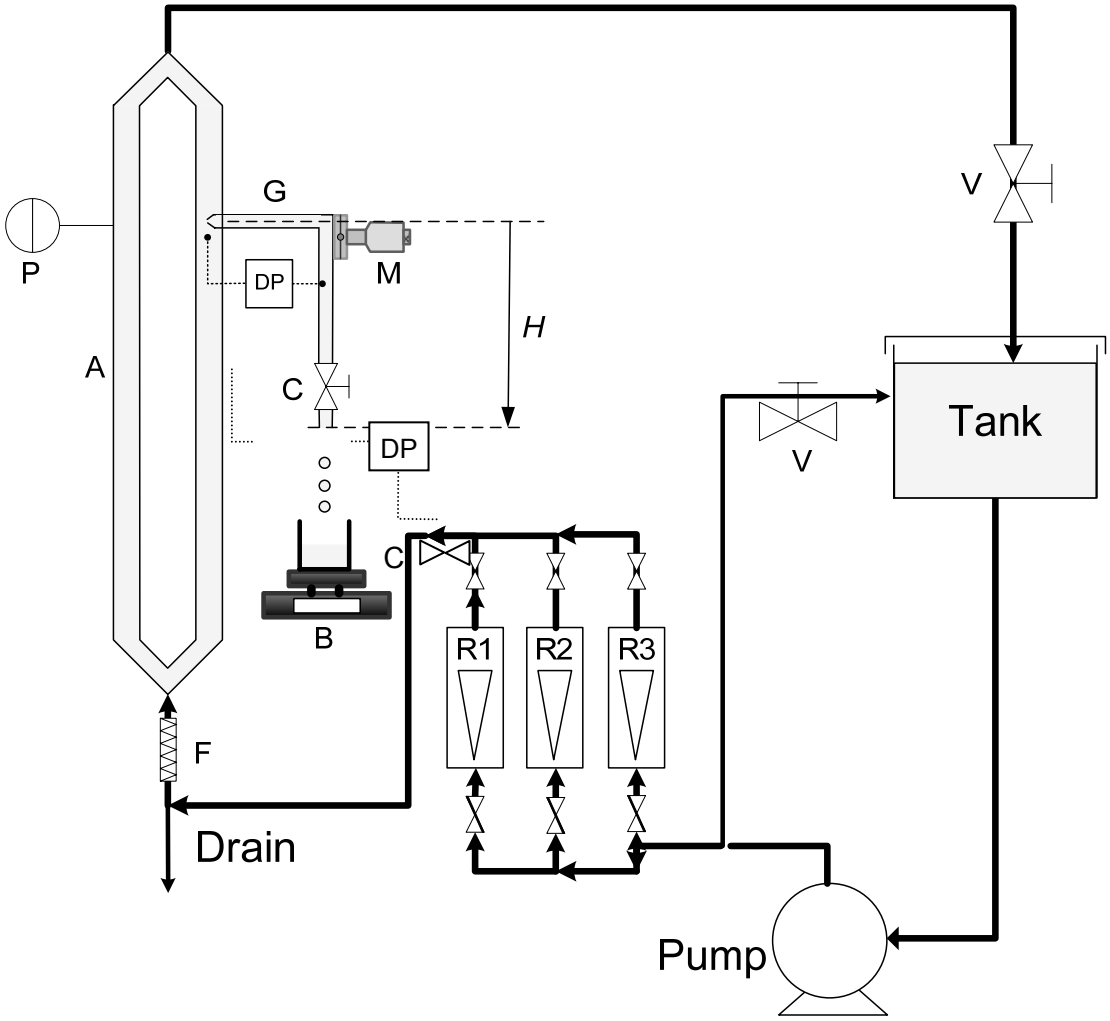

Figure 2: Schematic of apparatus 1: A - annular test section; B - electronic balance; C - gauging flow control valve; DP - differential pressure cell; F - filter; G - gauging tube; *H* - hydrostatic head; M - micrometer; P - pressure sensor; R-flowmeter; V - bulk flow control valve.

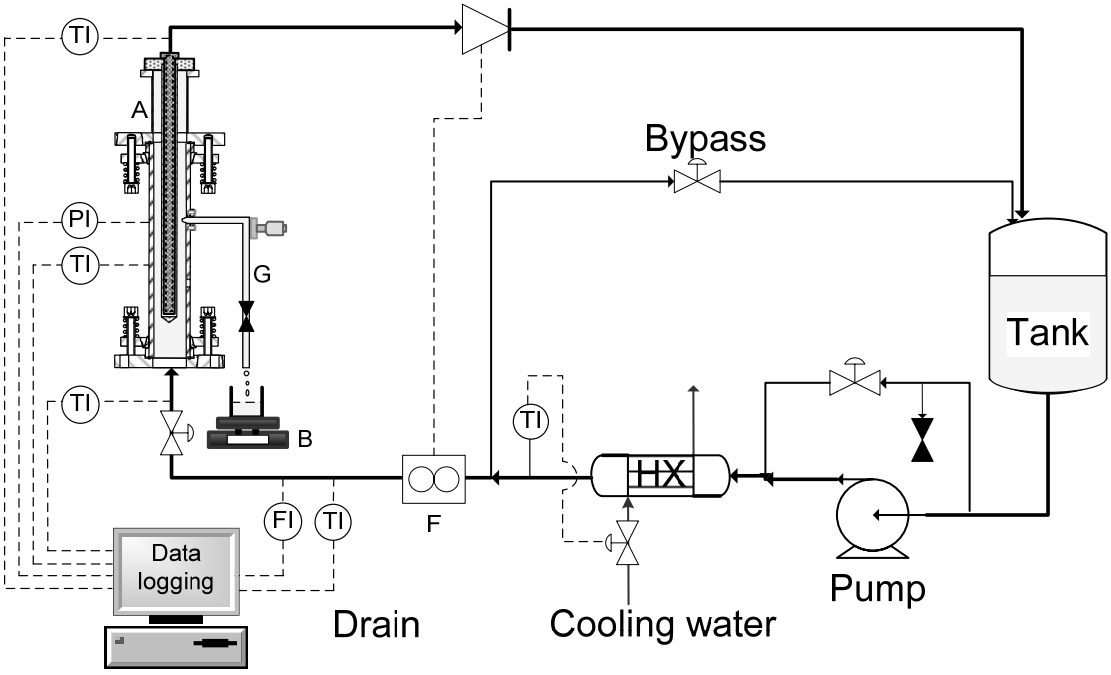

Figure 3: Schematic of apparatus 2: A - annular test section; B - electronic balance; F – flow controller; FI - flow indicator; G - gauging tube; HX - heat exchanger; PI - pressure sensor, TI - temperature sensor.

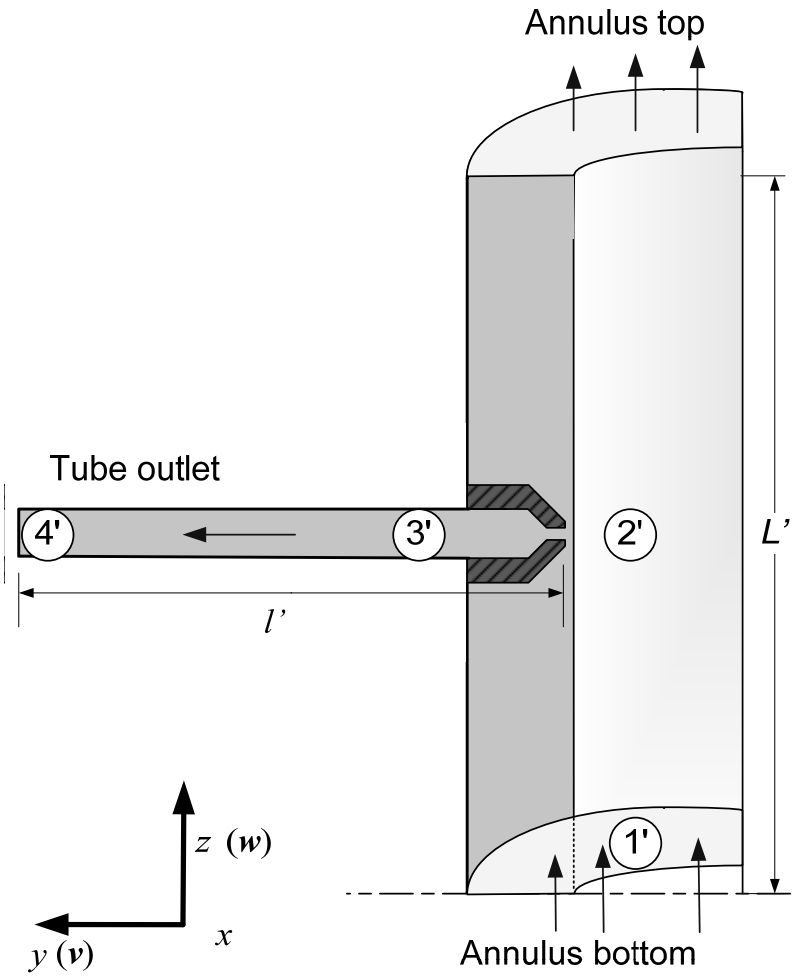

Figure 4: Simulation geometry. Numbers refer to the stations in the simulation. The arrows indicate the entry flow in the annulus, and the exit flow in the tube and annulus top. Co-ordinates: z - vertical (annulus) axis; y - horizontal (gauging tube) axis. Velocity components w and v are indicated.

(a)

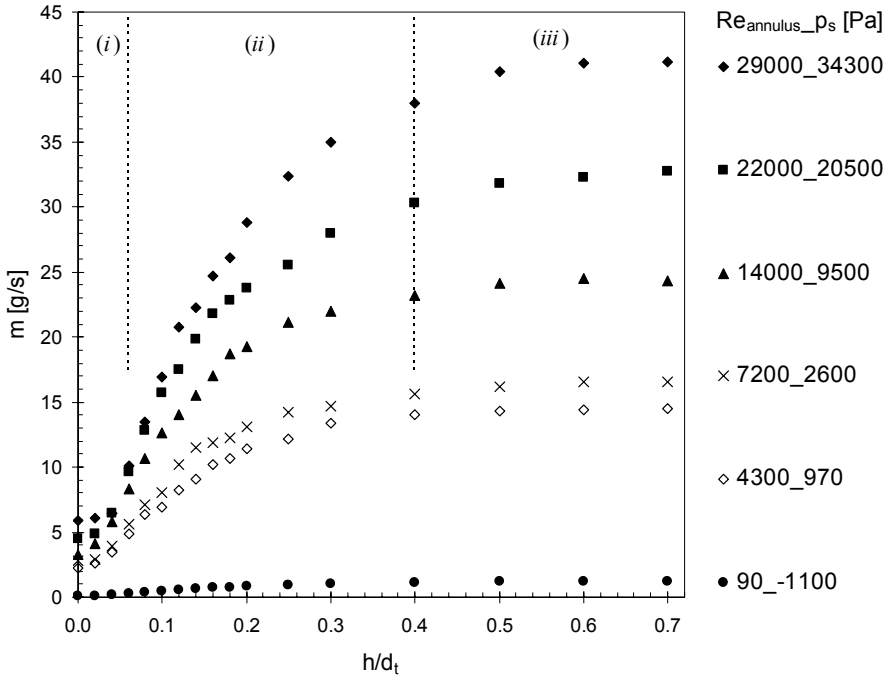

(b)

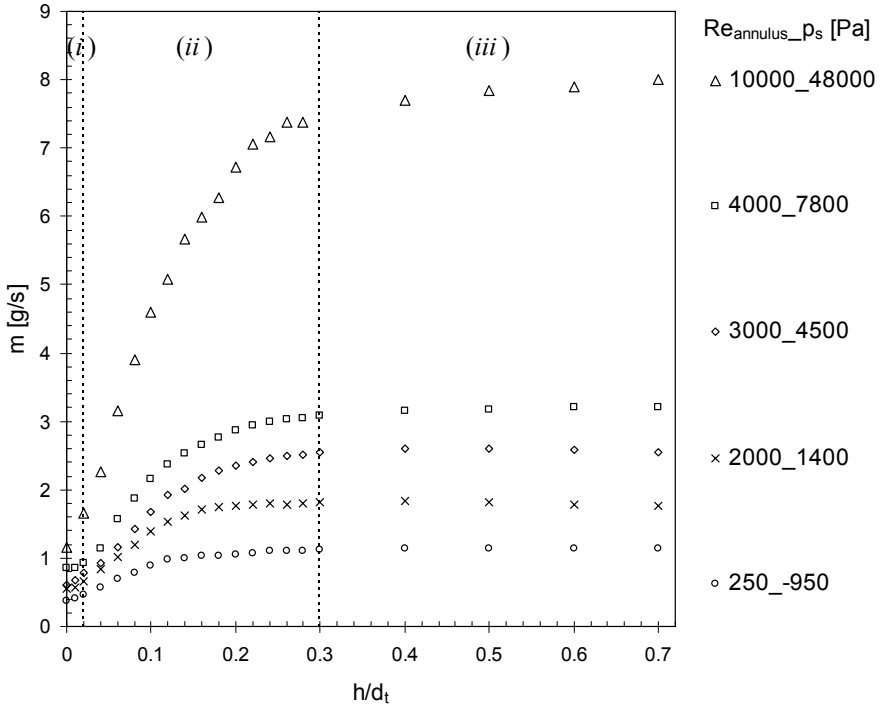

Figure 5: Effect of $Re_{annulus}$ on experimental FDG mass profile. Regions marked: (*i*) *curvature* zone; (*ii*) *incremental* zone; (*iii*) *asymptotic* zone. (*a*) Apparatus 1, $\alpha = 45°$, $H = 405$ mm; (*b*) Apparatus 2, $\alpha = 30°$, $H = 350$ mm. (*c*) Data replotted as dimensionless mass flow rate – clearance profiles; solid symbols, Apparatus 1, open symbols Apparatus 2.

(c)

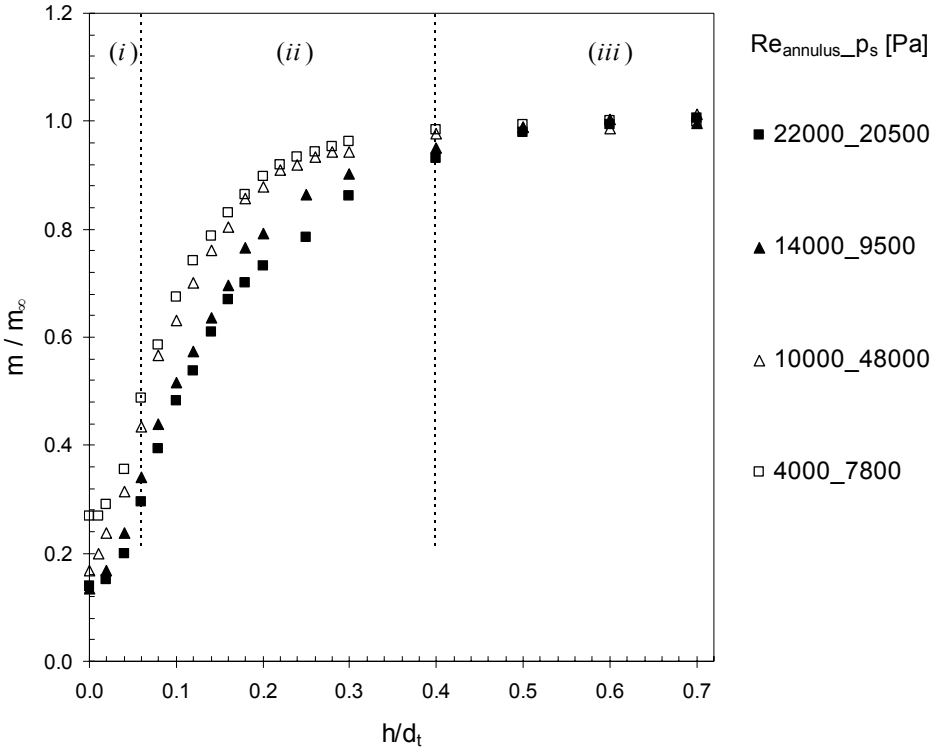

Figure 5: Effect of $Re_{annulus}$ on experimental FDG mass profile. Regions marked: (*i*) *curvature* zone; (*ii*) *incremental* zone; (*iii*) *asymptotic* zone. (*a*) Apparatus 1, $\alpha = 45°$, $H = 405$ mm; (*b*) Apparatus 2, $\alpha = 30°$, $H = 350$ mm. (*c*) Data replotted as dimensionless mass flow rate – clearance profiles; solid symbols, Apparatus 1, open symbols Apparatus 2.

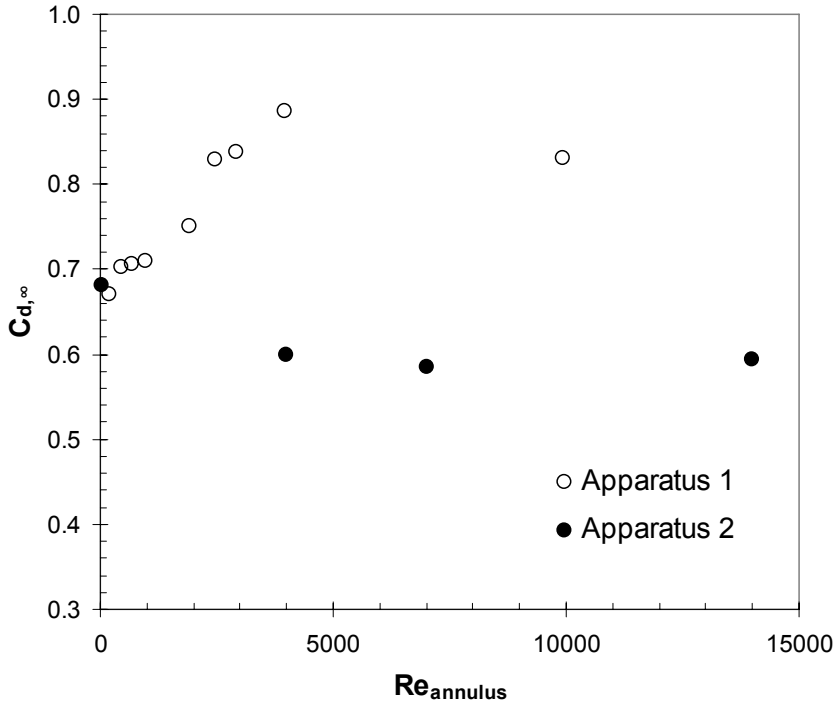

Figure 6: Effect of $Re_{annulus}$ on asymptotic nozzle discharge coefficient $C_{d,\infty}$ for gauge in apparatus 1 and 2, respectively. Solid circles: gauge 1; open circles: gauge 2.

(a)

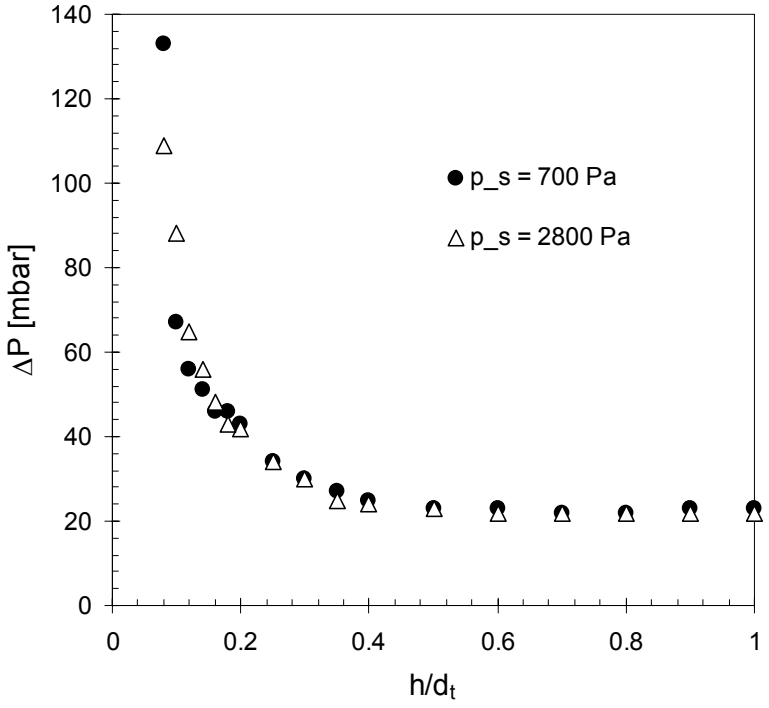

(b)

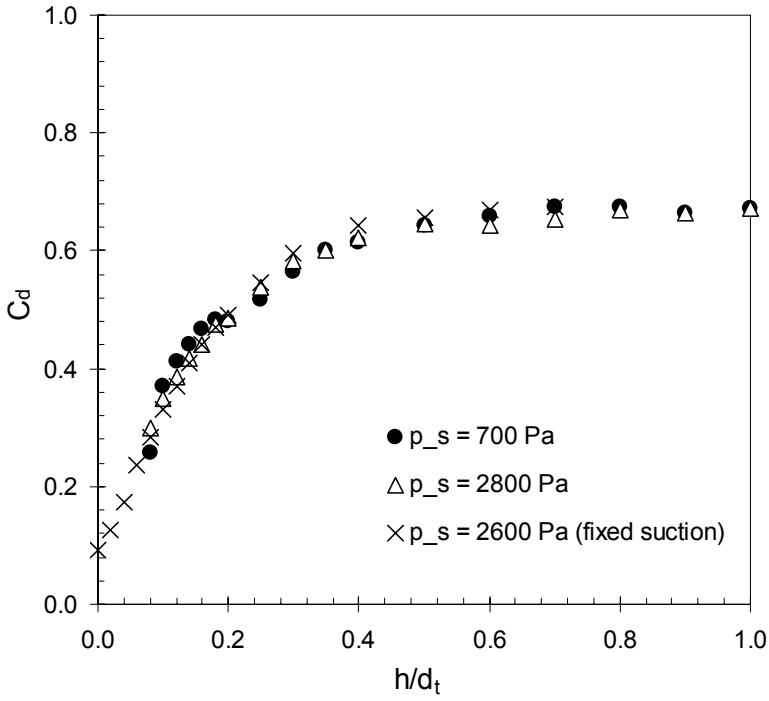

Figure 7: Fixed gauging flow rate mode, apparatus 1: (*a*) effect of h/d_t on pressure drop across the gauging nozzle, $Re_{annulus}$ = 1100, m ~ 1.1 g/s; (*b*) discharge coefficient. Circles - p_s = 700 Pa, triangles - p_s = 2800 Pa, crosses - data set from fixed suction mode, $Re_{annulus}$ = 1100, p_s = 2600 Pa.

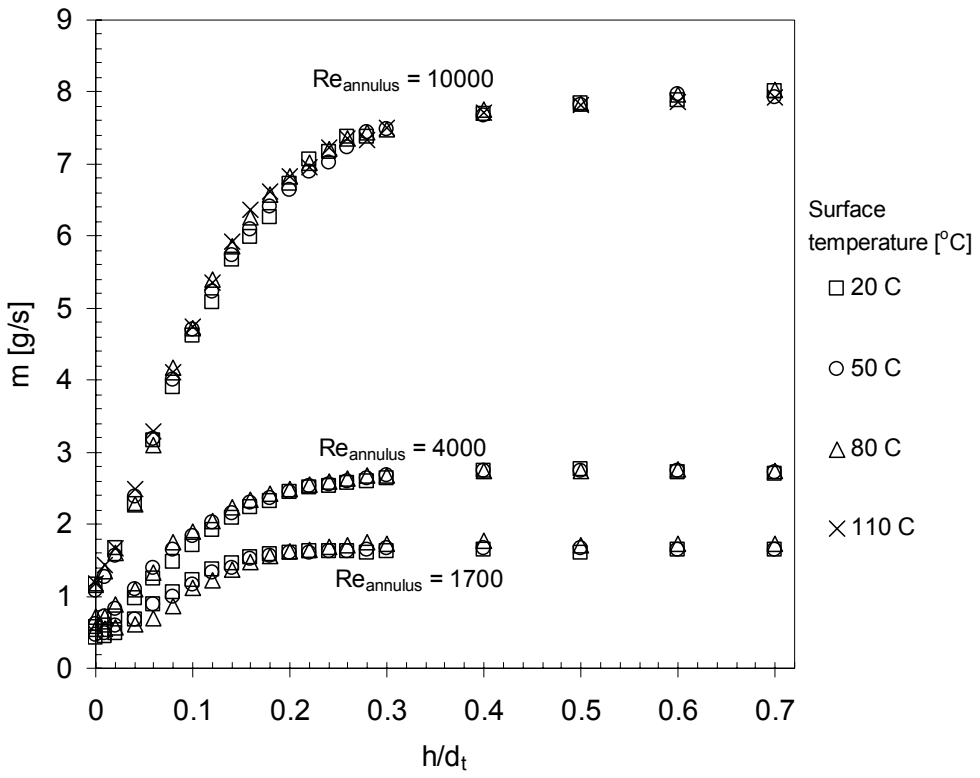

Figure 8: Effect of wall temperature on discharge mass flow rate. Apparatus 2, fixed suction operating mode. Bulk flow temperature, 20 °C, H = 350 mm. Symbols: squares - surface temperature = 20 °C; circles, 50 °C; triangles, 80 °C; crosses, 110 °C.

(a)

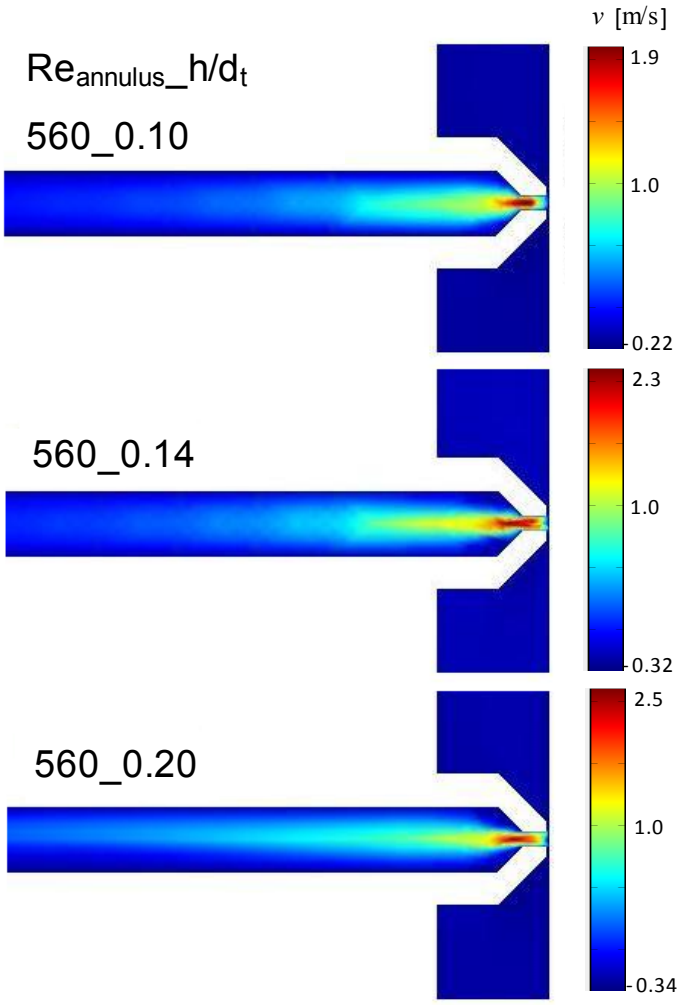

Figure 9: Simulated tube (y-wise) velocity component at the y-z plane of symmetry for apparatus 1, at $Re_{annulus}$ values of (a) 560 and (b) 90. The simulation shows that the maximum y-wise velocity occurs at the nozzle throat.

(b)

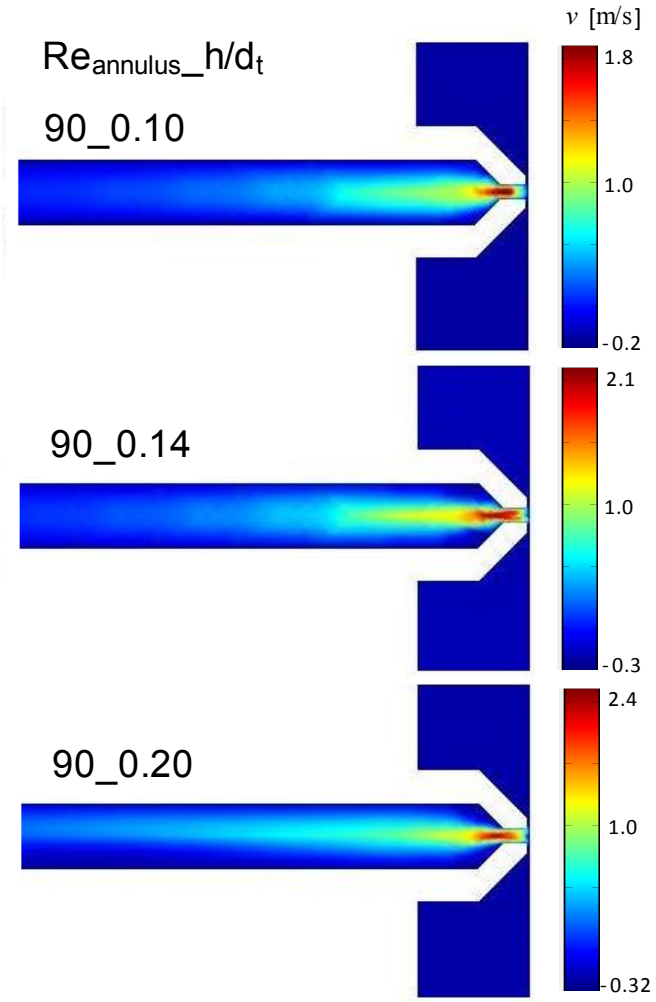

Figure 9: Simulated tube (*y*-wise) velocity component at the *y*-*z* plane of symmetry for apparatus 1, at $Re_{annulus}$ values of (*a*) 560 and (*b*) 90. The simulation shows that the maximum *y*-wise velocity occurs at the nozzle throat.

(a)

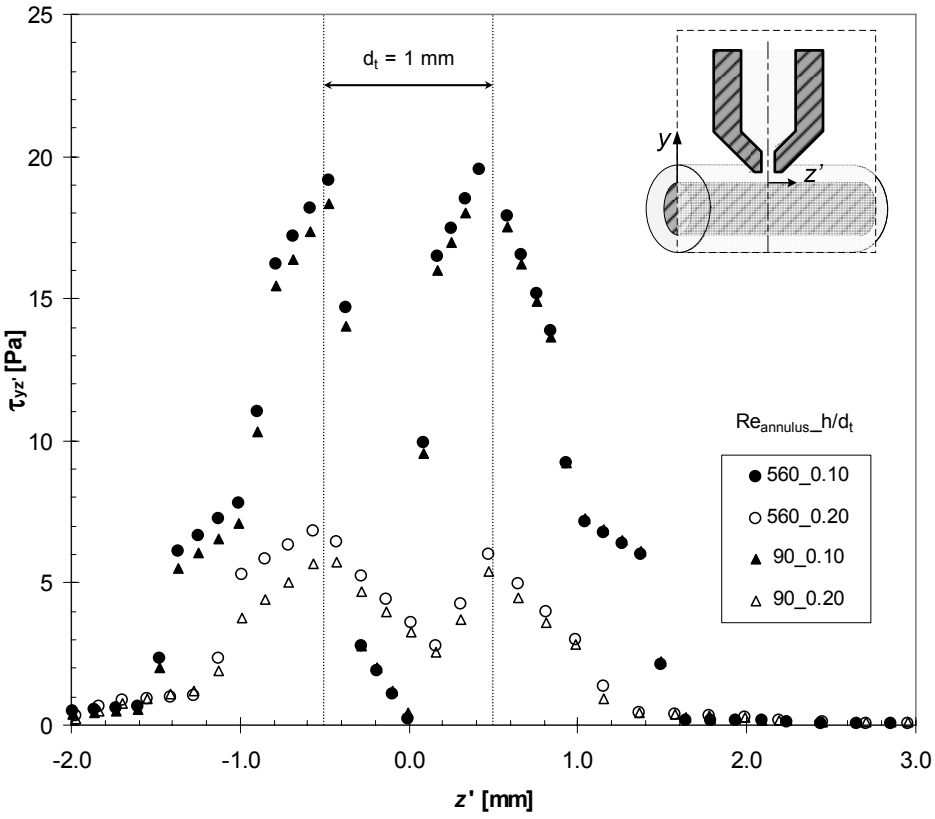

Figure 10: Shear stresses imposed by the gauging flow on the inner surface of the apparatus 1 annulus (*i.e.* at $y = 0$), directly underneath the gauge, as illustrated in the insets. (*a*) stress along the inner surface of the annulus in the z'-direction, $\tau_{yz'}$. (*b*) Shear stress, τ_{ya}, imposed by the gauging flow on the inner surface of the annulus at different positions along the arc, a.

(b)

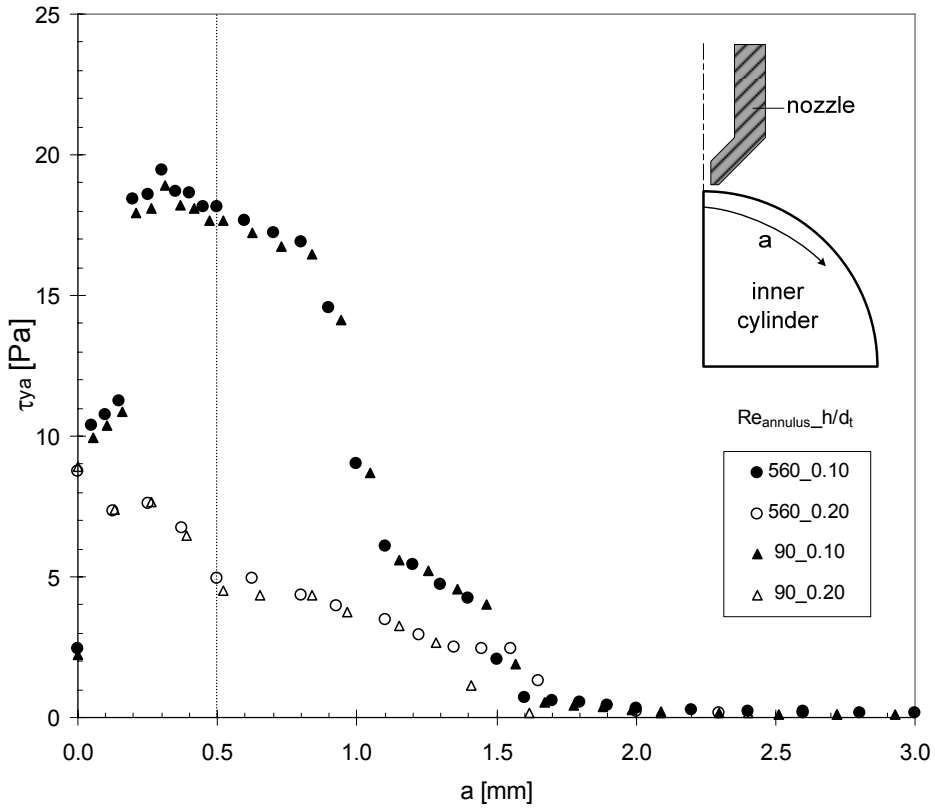

Figure 10: Shear stresses imposed by the gauging flow on the inner surface of the apparatus 1 annulus (*i.e.* at $y = 0$), directly underneath the gauge, as illustrated in the insets. (*a*) stress along the inner surface of the annulus in the z'-direction, $\tau_{yz'}$. (*b*) Shear stress, τ_{ya}, imposed by the gauging flow on the inner surface of the annulus at different positions along the arc, a.

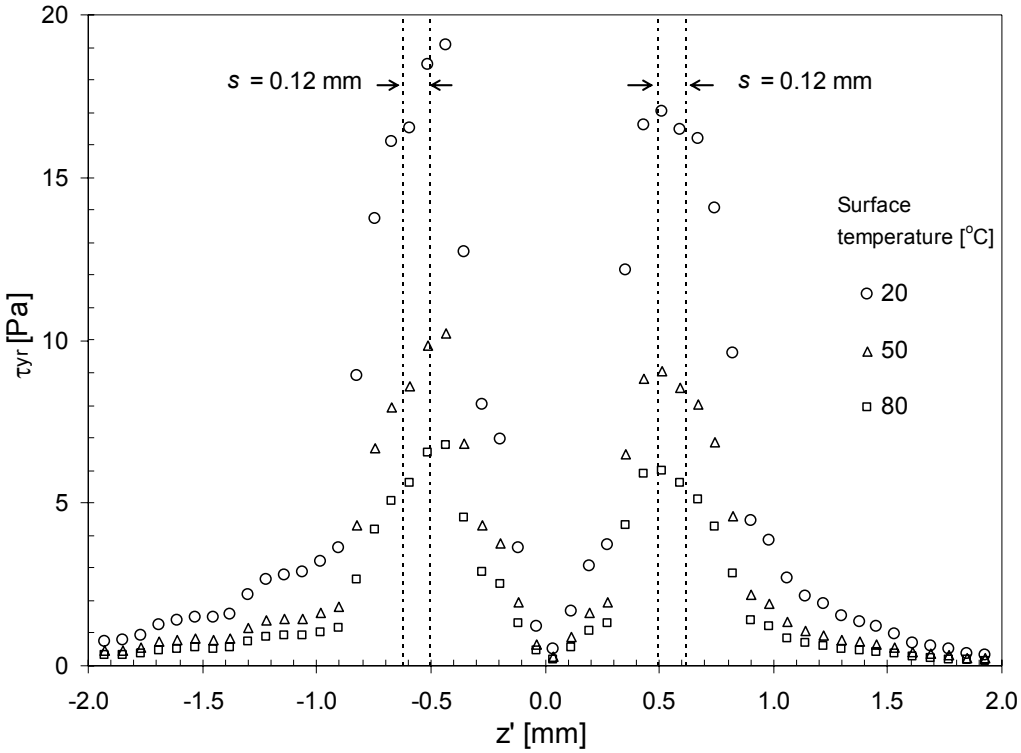

Figure 11: Heated surface annular flow mode FDG (apparatus 2): Shear stress imposed by the gauging flow on the inner convex surface of the annulus (at $y = 0$), as a function of the annulus axial coordinate measured from the gauge central axis. Conditions: $Re_{\text{annulus}} = 1700$, $Re_{\text{tube}} = 500$, $p_s = -920$ Pa, $h/d_t = 0.18$. Circles, 20 °C; triangles, 50 °C; squares, 80 °C.

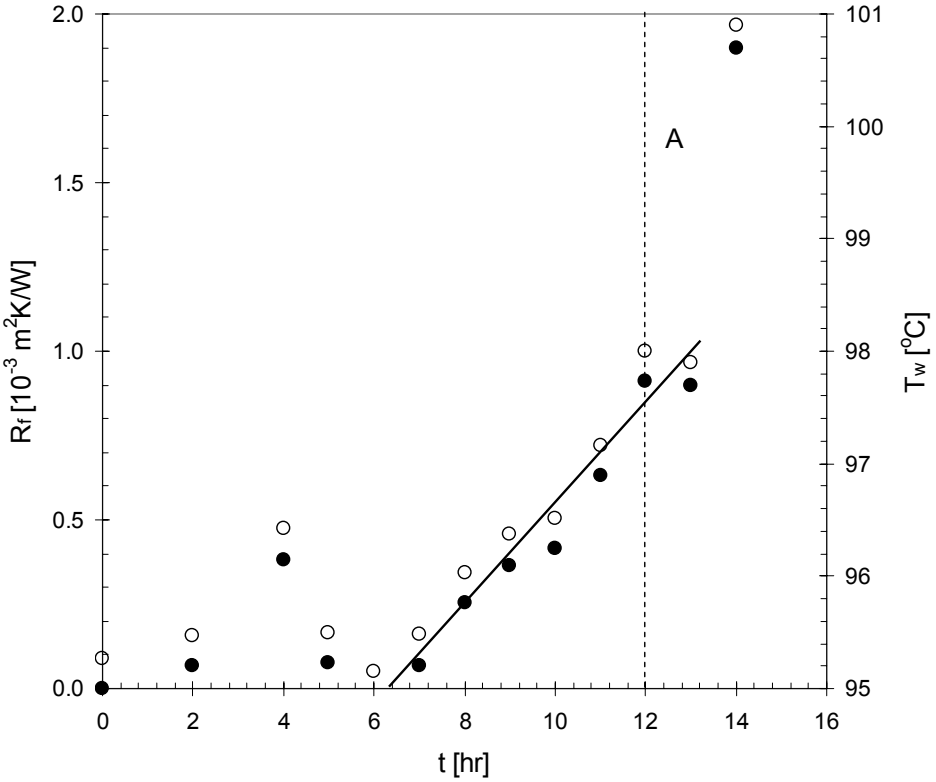

Figure 12: Fouling in 3.5 wt% WPC solution using apparatus 2 (experiment 1). Experimental conditions: $Re_{annulus}$ = 7300, T_{bulk} = 53 °C, p_s = 7580 Pa, pH = 6. Symbols: square – T_w; diamonds - R_f. Error bar is represented by the size of the symbols. Vertical dashed line at A marks the time at which FDG measurements were made. Solid locus - linear regression to initial growth data, giving R_f (in m^2K/W) = 1.5×10^{-4} t (in hr) – 1.02. R^2 = 0.95.

Figure 13: Images of the ring left by the gauging nozzle (*a*) *in-situ*, after fouling experiment 1; (*b*) *ex-situ*, using a digital microscope under 50× magnification.

Table 1: Mesh refinement result for the simulation case $h/d_t = 0.1$, $Re_{annulus} = 90$, $Re_{tube} = 150$.

N_e	$C_{d,\,sim}$	$C_{d,\,exp}$	% *diff.*	Computational time (min)
6124	0.259		– 0.49	18
5680	0.263	0.258	– 2.07	14
4956	0.273		– 5.81	12

Table 2: Summary of CFD simulation of FDG in annular flow (apparatus 1), isothermal case.

h/d_t	$Re_{annulus}$	$C_{d,exp}$	$C_{d,sim}$	% *diff.*	Re_{tube}
0.10		0.266	0.240	10%	542
0.14	560	0.364	0.347	5%	740
0.20		0.481	0.473	2%	973
0.10		0.261	0.240	8%	532
0.14	300	0.353	0.347	2%	718
0.20		0.476	0.472	1%	964
0.10		0.264	0.240	9%	538
0.14	190	0.351	0.362	-3%	714
0.20		0.472	0.472	0%	956
0.10		0.258	0.240	7%	527
0.14	90	0.342	0.350	-1%	696
0.20		0.465	0.472	-2%	941